ADVANCES IN ATMOSPHERIC SCIENCES, VOL. 32, NOVEMBER 2015, 1533–1538

Bred Vectors of the Lorenz63 System

Ying ZHANG*, Kayo IDE, and Eugenia KALNAY

Department of Atmospheric and Oceanic Science, University of Maryland, College Park, Maryland, USA

(Received 14 December 2014; revised 10 April 2015; accepted 6 May 2015)

ABSTRACT

The breeding method has been widely used in studies of data assimilation, predictability and instabilities. The bred vectors (BVs), which are the nonlinear difference between the control and perturbed runs, represent the time-evolving rapidly growing errors in dynamic systems. The Lorenz (1963) model (hereafter Lorenz63 model) has chaotic dynamics similar to weather and climate. This study investigates the features of BVs of the Lorenz63 model and its impact on regime prediction of the Lorenz63 model. The results show that the Lorenz63 model has two different BVs for each breeding cycle, and the two BVs approach being identical when growth rate is high. The duration of the current and next regime is associated with the relative directions between the BV with high growth rate and the model trajectory.

Key words: bred vectors, chaos, Lorenz63 model, regime prediction

Citation: Zhang, Y., K. Ide, and E. Kalnay, 2015: Bred vectors of the Lorenz63 system. *Adv. Atmos. Sci.*, **32**(11), 1533–1538, doi: 10.1007/s00376-015-4275-8.

1. Introduction

The breeding method proposed by Toth and Kalnay (1993, 1997) is designed to estimate dynamic forecast errors and produce perturbations for ensemble forecasting. The steps of breeding are adding a small random initial perturbation to a control run, integrating forward, and periodically rescaling the difference between the perturbed and control runs to the size of initial perturbation at the end of each fixed rescaling interval. The difference between the perturbed and control runs is called the bred vector (BV) and the process during a fixed rescaling interval is called a breeding cycle.

The breeding method generates time-evolving perturbations in directions where errors have grown fast. It is easy to apply and computationally inexpensive, and thus it has been used not only in data assimilation (e.g., Kalnay, 2003; Yang et al., 2006; Yang et al., 2009) but also in other applications. For example, it has been used for producing initial perturbations for operational ensemble forecasts at the National Centers for Environmental Prediction (NCEP) since December 1992 (Toth and Kalnay, 1997). Besides this, it was employed to study the "error of the day" (e.g., Kalnay and Toth, 1994; Kalnay, 2003), to investigate the structure of background error covariance (Corazza et al., 2003; Yang et al., 2009), and to discover the intrinsic predictability and instabilities of chaotic systems, such as the atmosphere of Mars (Newman et al., 2003; Greybush et al., 2013), baroclinic rotating annulus (Young and Read, 2008), and global upper ocean (Hoffman et al., 2009).

* Corresponding author: Ying ZHANG
Email: yzhang@atmos.umd.edu

The Lorenz (1963) model (hereafter Lorenz63 model) was designed to represent forced dissipative hydrodynamic flow. The equations of the model are

$$\begin{cases} \dfrac{dx}{dt} = a(y-x) \,, \\ \dfrac{dy}{dt} = rx - y - xz \,, \\ \dfrac{dz}{dt} = xy - bz \,, \end{cases}$$

where the original values $a = 10, b = 8/3$ and $r = 28$ are chosen for chaotic behavior (Lorenz, 1963). The trajectory of the Lorenz solutions in three-dimensional (3D) phase space exhibits a "butterfly" shape and the two wings of the butterfly attractor are regarded as "warm" ($x > 0$ and $y > 0$) and "cold" ($x < 0$ and $y < 0$) regimes, respectively. Transitions between the two regimes take place aperiodically. The solutions of the equations are also nonperiodic and sensitive to small changes in initial conditions. Hence, due to its chaotic dynamics, similar to those of weather and climate, this model has been widely used for predictability studies in meteorology.

Evans et al. (2004) studied the possible prediction of regime transitions in the Lorenz63 model using breeding and found two rules: (1) regime transitions happened after the appearance of high BV growth rate [indicated by the red stars in Fig. 4 of Evans et al. (2004)], and (2) the duration of the new regime was proportional to the number of red stars [as shown in Fig. 5 of Evans et al. (2004)]. This study was carried out on the basis of one BV for each breeding cycle. However, is it possible that this 3D model has more than one BV for each

breeding cycle? Moreover, if so, do they perform differently in predicting regime transitions? These questions have not been previously studied.

The goal of the present study is to examine whether the Lorenz63 system has more than one BV for each breeding cycle and how those BVs affect the prediction of regime transitions. The remainder of the paper is organized as follows: The experiment design is described in section 2. In section 3, we examine whether the Lorenz63 system has more than one BV for each breeding cycle and the impacts of those BVs on predicting regime transitions. Finally, the results are summarized in section 4.

2. Experiment design

There are three key parameters in breeding: the rescaling interval, size of initial perturbation, and direction of initial perturbation. In the nonlinear breeding method, the perturbation initially grows linearly and then becomes saturated. Hence, for a short rescaling interval and/or small initial perturbation, the linear growth dominates; whereas, for a long rescaling interval and/or large initial perturbation, the linear growth of the perturbation will saturate and then nonlinear growth will dominate.

The Lyapunov exponents (LEs), which quantitatively estimate the stability properties of a dynamic system, are 0.906, 0, and -14.572 for the Lorenz63 system under the given parameters (Wolf et al., 1985; Wolfe and Samelson, 2007). The first positive LE is associated with the leading Lyapunov vector and the second LE with the second Lyapunov vector. When an instability exists in a system, all initial perturbations will converge to the fastest-growing leading Lyapunov vector. The Lyapunov vectors with finite amplitude in finite time, i.e. local Lyapunov vectors (LLV), could be extended nonlinearly by several methods, such as BVs (Kalnay and Toth, 1996) and the nonlinear local Lyapunov vectors (Feng et al., 2014) oriented from the nonlinear local Lyapunov exponent (Ding and Li, 2007; Li and Wang, 2008; Li and Ding, 2011).

In order to check how many BVs the Lorenz63 model has for each breeding cycle, a series of sensitivity experiments has been designed by randomly changing the direction of initial perturbation but fixing the rescaling interval to eight time steps ($dt = 0.01$ is one time step) and the size of the initial perturbation to 1 for primary focus. If there is only one BV for each breeding cycle, i.e., one leading LLV (Kalnay and Toth, 1996; Kalnay, 2003), no matter which direction you add to the initial perturbation, after a finite period, all the perturbations will converge to the direction of the leading LLV or, equivalently, its opposite direction. Otherwise, perturbations might not merge into just one direction. The direction of the initial perturbation has been altered 14 times, so as to cover most of the 3D space. The model has been integrated for a long time for all the 14 experiments, after spinning up hundreds of time steps from its initial position. Two series of similar sensitivity experiments with the same 14 initial perturbations but shorter rescaling intervals (four and two time steps) and smaller amplitudes of initial perturbations (0.5 and 0.1) have also been carried out to represent more linear cases, in which the BVs have less nonlinear growth than in the primary experiments. The results reported below are from the primary experiments unless otherwise stated.

3. Results

3.1. *Case of two BVs for each breeding cycle existing in the Lorenz63 system*

The BV growth rates of the 14 experiments merge into two lines after integrating several hundred time steps: ten of them merge into one line and the other four merge into the other line. Hence, 14 BVs for each breeding cycle in these experiments converge towards two BVs, denoted by BV1 and BV2 respectively. All BV1s and BV2s in the figures are composited of the ten BV1 experiments and of the four BV2 experiments, respectively.

The 3D attractors with both BV1 and BV2 colored with their growth rates are shown in Figs. 1a and b. The BV for every breeding cycle (i.e., every eight time steps) is indicated by a line segment originating from a filled colored circle on the trajectory and its direction is from the filled colored circle on the trajectory to the unfilled black one. The arrows denote the moving direction of the trajectory. One difference between the two figures is obvious; that is, for each breeding cycle, the BV1 points to different directions from the corresponding BV2 and they tend to be opposite when the colored head is red (growth rate > 6.4), even on the same trajectory. To clearly present this difference, a few BV1s (denoted by thick line segments) at the bottom of the warm regime are added in Fig. 1b. Hence, it is suggested that BV1 and BV2 are distinct; otherwise, they would point to exactly the same or opposite directions.

In order to further verify if BV1 and BV2 for each breeding cycle really are two different BVs, the exact angle between them during the whole integration period is calculated, as shown in Fig. 2a. None of the angles (colored with the growth rate of BV1) exactly equals 0° or 180°, even for more linear cases (shorter rescaling interval and smaller initial perturbation). Overall, the angle evolves closer to 180° for more linear cases. Hence, for each breeding cycle, BV1 and BV2 are not identical, but are two different vectors. In addition, almost all the red stars occur nearest to 180°. This proves that BV1 and BV2 with high growth rates (> 6.4) tend to head in opposite directions in Fig. 1, i.e., they tend to become identical (except for the sign), as exemplified by the black rectangle in Fig. 1b.

Furthermore, examining the ensemble dimension (i.e., E-dimension) of the Lorenz63 model is another way to prove that BV1 and BV2 are different. The E-dimension, which was introduced by Patil et al. (2001) and further examined by Oczkowski et al. (2005), gives the effective number of dominant directions in the subspace spanned by an M-member set of perturbations at a given time:

$$E = \frac{(\sum_{m=1}^{M} s_m)^2}{\sum_{m=1}^{M} s_m^2},$$

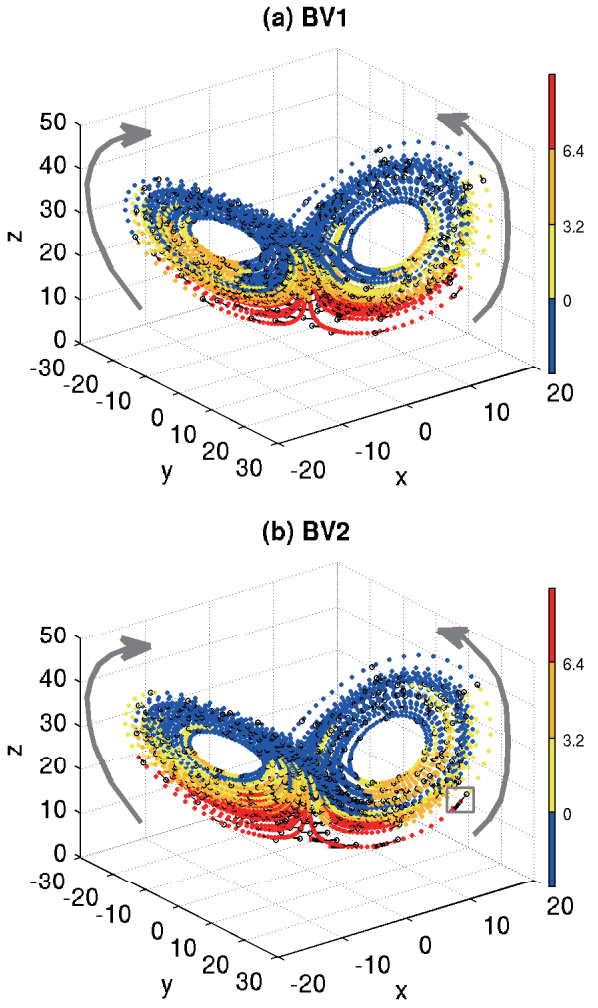

Fig. 1. 3D Lorenz 63 attractor colored with growth rate (color bar) and BVs for each breeding cycle. Blue represents a BV growth rate < 0, yellow for $0 \leqslant$ growth rate < 3.2, orange for $3.2 \leqslant$ growth rate < 6.4, and red for growth rate $\geqslant 6.4$: (a) BV1; (b) BV2. Thick line segments at the bottom of the attractor in the warm regime indicate the corresponding BV1 for these breeding cycles. The arrows represent the direction of the model trajectory. The grey rectangle indicates an example of a high-growth BV1 (thick line segment) and a high-growth BV2 (thin line segment) being close to 180° at a breeding time step.

where s_m is the m-th singular value of the matrix constructed by the M local bred vectors in descending order. The $E = 1$ case indicates the perturbations are confined to a single direction; while the $E = M$ case means the uncertainty is evenly distributed in M directions. The E-dimension of the Lorenz63 system using the initial perturbations selected in the 14 experiments is colored with the BV growth rate averaged for the 14 experiments and presented in Fig. 2b. The E-dimension is less than 2 but greater than 1 during the entire integration period, and it is closer to 1 for the more linear cases in which the rescaling interval is four or two time steps and the initial amplitude is 0.5 or 0.1. This confirms that the BVs in the Lorenz63 model have converged into two dominant directions and they approach one direction in more linear cases. Moreover, nearly all red stars occur when the E-dimension approaches 1. This again verifies that BV1 and BV2 for each breeding cycle in the 14 experiments tend to become identical when growth rates exceed 6.4. After high growth rate occurs, the angle does not suddenly drop far away from 180°, but gradually decreases, as does the E-dimension.

Figure 2c, which is a scatter plot of the E-dimension and the angle between BV1 and BV2, shows an apparent parabolic pattern: the E-dimension is closest to 2 when BV1 is perpendicular to BV2 (angle = 90°), and it is closest to 1 when BV1 is nearly opposite/parallel to BV2 (indicated by the red rectangular box). This implies that BV1 and BV2 approach being identical not only during the high growth rate period, but also afterwards. The approximate parabolic pattern is broken in more linear cases, since BV1 and BV2 become more identical and the scatters are concentrated around the red rectangular box in Fig. 2c. Hence, the nonlinear growth of BVs is necessary to allow BVs to grow in more than one direction.

When comparing the evolutions of the angle and E-dimension with that of x, which denotes regime duration and transitions, it seems that the angle drops away from 180° and the E-dimension stays near 2 when the regime lasts for a long time; while the angle stays near 180° and the E-dimension is close to 1 when the duration of the regime is short.

Therefore, it can be concluded that the Lorenz63 system has two BVs for each breeding cycle and that the two BVs tend to become identical (i.e., the angle between BV1 and BV2 is close to 180°) when they have high growth rate. This is complementary to the findings of Norwood et al. (2013), that the leading Lyapunov vector of the Lorenz63 system, LV1, grows fastest globally; the second Lyapunov vector, LV2, does not grow globally but usually grows faster than LV1 locally. BVs, which are associated with the LLV, grow towards the fastest growing local Lyapunov vector. Normally, the BV is parallel to the LV1, but when the LV2 grows faster than LV1 locally, the BV becomes parallel to the LV2.

3.2. *Impacts of BV1 and BV2 on predicting regime transitions*

Evans et al. (2004) discovered the fast-growing BV is a predictor for regime transitions of the Lorenz63 model. The above analysis has indicated that the Lorenz63 model has two BVs for each breeding cycle and, thus, the impacts of this finding on predicting regime duration and transitions are worth exploring.

Regime transitions include transitions from warm to cold regime and those from cold to warm regime. However, if these two types of transitions are not separated as in Evans et al. (2004), there is no obvious distinction between the predictions of the two BVs with high growth rate for each breeding cycle. Actually, in Fig. 1, BV1s with high growth rate (indicated by red dots) are dragged by the trajectory in the warm regime but forward along the trajectory in the cold regime; while the situation is opposite for BV2. Hence, the two BVs might perform differently in terms of prediction when the two types of transitions are considered separately.

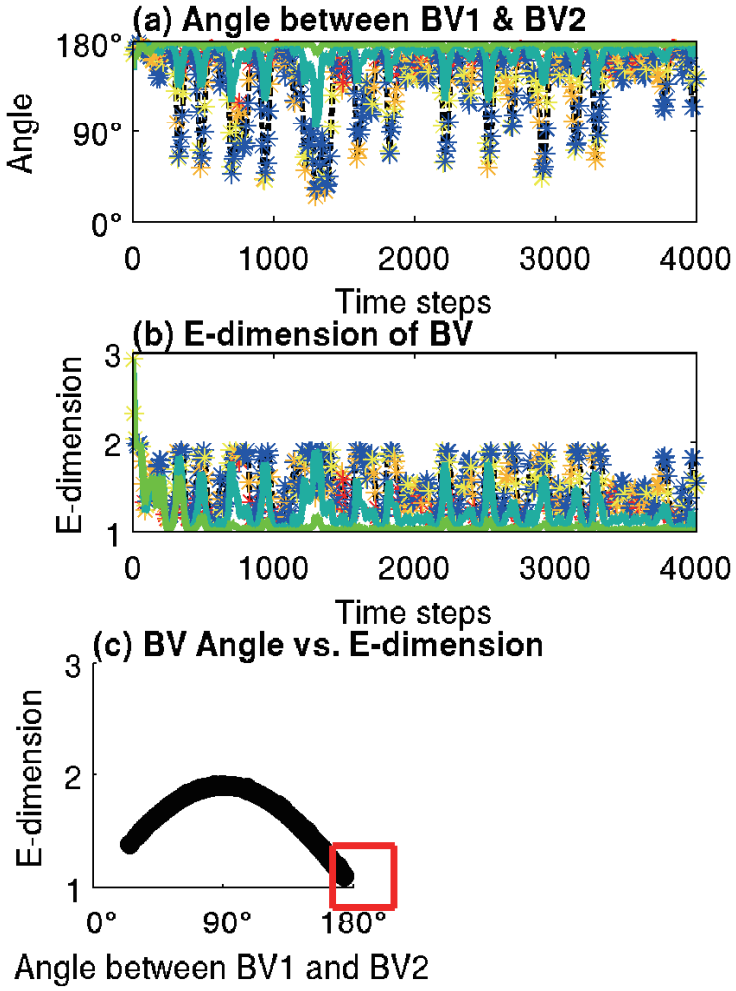

Fig. 2. (a) Angles between BV1 and BV2, colored with the growth rate of BV1. (b) E-dimension colored with mean growth rate of BV1 [dashed line with colored stars indicates the breeding experiments with the rescaling interval equal to eight time step (Tw = 8*dt*) and the size of the initial perturbation equal to 1 ($\sigma = 1$); turquoise line for experiments with Tw = 4*dt* and $\sigma = 0.5$; and green line for experiments with Tw = 2*dt* and $\sigma = 0.1$]. (c) Relationship between the BV1–BV2 angle and *E*-dimension for the experiments with Tw = 8*dt* and $\sigma = 1$. The red rectangular box indicates the convergence of BV1 and BV2 to a single BV.

Figure 3 shows the prediction of transitions from warm to cold regime and from cold to warm regime by BV1 and BV2. For the same number of red stars (BVs with high growth rate) in warm regimes, the next cold regime predicted by BV1 in the warm regime (opposite to the direction of the model trajectory) will last for a shorter time than that by BV2 in the warm regime (in the same direction as the model trajectory). Conversely, for the same number of red stars in cold regimes, the next warm regime predicted by BV1 in the cold regime (in the same direction as the model trajectory) will last for a longer time than that by BV2 in the cold regime (opposite to the direction of the model trajectory). This indicates that the length of the next regime is associated with the relative direction between the high-growth BV and the moving trajectory. For the total number of red stars, more high-growth BVs are found when their directions are against the direction of the model trajectory, such as BV1 in warm regimes, shown by grey circles in Fig. 3a, and BV2 in cold regime, shown by black crosses in Fig. 3b. This is also consistent with more red dots in the warm regime than in the cold regime in Fig. 1a, and more red dots in cold regimes than in warm regimes in Fig. 1b. This implies a longer duration of the current regime when more high-growth BVs point in the opposite direction to the model trajectory.

Lorenz (1963) found that if the value of maximum *z* is gradually increasing in one regime then the trajectory will move to another regime after the value of maximum *z* reaches a critical value. This finding is also supported by the value of

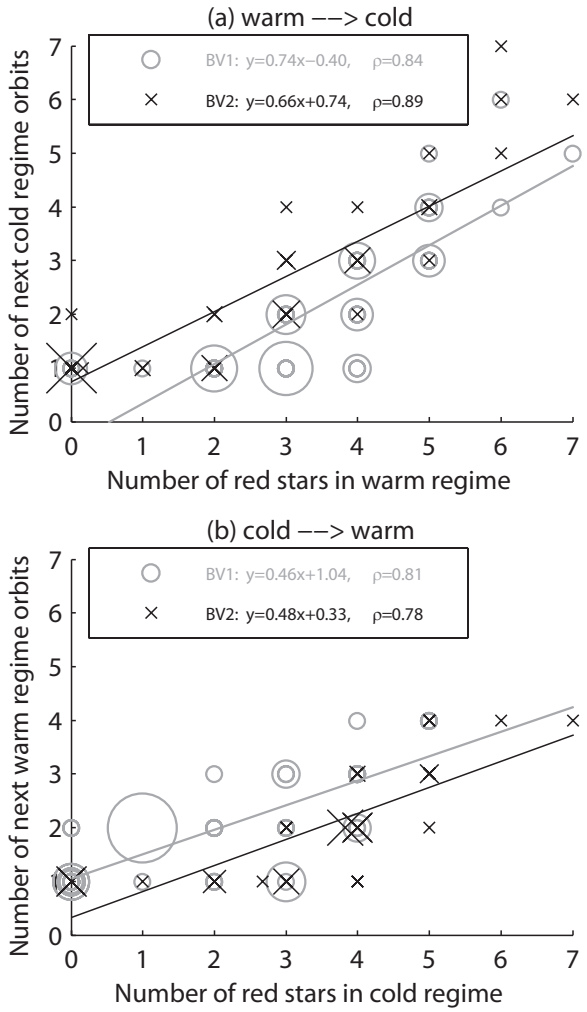

Fig. 3. Prediction of regime transitions (indicated by the number of orbits in the next regime) by numbers of red stars (BVs with high growth rate) for BV1 and BV2 in a regime. The size of the circles and crosses reflects the number of corresponding pairs: (a) Regime transition from warm to cold; (b) regime transition from cold to warm.

minimum z: if the value of minimum z is gradually decreasing in one regime, up until reaching a critical value, a regime transition will subsequently take place. The relationship between the regime duration and the directions of high-growth BVs and the trajectory could be explained by the finding in Lorenz (1963).

When the high-growth BV tends to align with the trajectory in the current regime, e.g., the red dots in the cold regime in Fig. 1a, it will fall in a high position (large value of minimum z, i.e., the blue dots at $z \in [10, 20]$ in the warm regime in Fig. 1a) and be dragged by the trajectory against the flow direction in the next regime, the current regime will have a short duration (e.g., BV1 in cold regimes and BV2 in warm regimes), and the next regime will have a long duration. Whereas, when the high-growth BV tends to be dragged by the trajectory in the current regime, e.g., the red dots in the warm regime in Fig. 1a, it will penetrate into a low position (small value of minimum z, i.e., the blue and yellow dots at $z \in [10, 20]$ in the cold regime in Fig. 1a) and follow the trajectory's direction in the next regime, the current regime will last a long time (e.g., BV1 in warm regimes and BV2 in cold regimes), and the next regime will last a short time.

Therefore, the two BVs perform differently in predicting regime transitions, considering the regime transitions from warm to cold and from cold to warm separately. When the direction of the BV with high growth rate is parallel (opposite) to the moving direction of the trajectory, the current regime will have a short (long) duration, and the next regime will have a long (short) duration.

4. Conclusions

This paper has explored the characteristics of BVs in the Lorenz63 model. By examining BV directions and E-dimensions, it has been found that that the chaotic 3D Lorenz63 model has two different BVs for each breeding cycle, and the two BVs tend to become identical when the growth rate is high. This indicates that, in nonlinear BV growth, initial perturbations from different arbitrary directions will converge into few different directions and the Lorenz63 model has two directions of nonlinear growing instability, which are both detected by the breeding method. The duration of the current regime is associated with the relative directions between the BV with high growth rate and the moving trajectory. If the two directions are the same (opposite), the current regime has a short (long) length and the next regime has a long (short) length.

Although this study has been performed using the simple 3D Lorenz63 system, it still has implications for nonlinear unstable perturbations in large systems. A nonlinearly growing perturbation may have more than one growing direction and the breeding method is capable of capturing nonlinear instabilities with different directions. The relative direction of the mean flow and the unstable perturbation is potentially useful for predicting regime transitions.

Acknowledgements. This work was jointly supported by the ONR (Office of Naval Research) (Grant No. N00014-10-1-0557), the Civil, Mechanical and Manufacturing Innovation Division of the NSF (National Science Foundation) (Grant No. CMMI112585), and NASA (National Aeronautic and Space Administration) (Grant No. 5069UMNASAMI3G).

REFERENCES

Corazza, M., and Coauthors, 2003: Use of the breeding technique to estimate the structure of the analysis "errors of the day". *Nonlinear Processes in Geophysics*, **10**, 233–243.

Ding, R. Q., and J. P. Li, 2007: Nonlinear finite-time Lyapunov exponent and predictability. *Physics Letters A*, **364**, 396–400, doi: 10.1016/j.physleta.2006.11.094.

Evans, E., N. Bhatti, L. Pann, J. Kinney, M. Peña, S.-C. Yang, E. Kalnay, and J. Hansen, 2004: RISE: Undergraduates find that regime changes in Lorenz's model are predictable. *Bull. Amer.*

Meteor. Soc., **85**, 520–524.

Feng, J., R. Q. Ding, D. Q. Liu, and J. P. Li, 2014: The Application of nonlinear local Lyapunov vectors to ensemble predictions in the Lorenz systems. *J. Atmos. Sci.*, **71**, 3554–3567.

Greybush, S. J., E. Kalnay, M. J. Hoffman, and R. J. Wilson, 2013: Identifying Martian atmospheric instabilities and their physical origins using bred vectors. *Quart. J. Roy. Meteor. Soc.*, **139**, 639–653, doi: 10.1002/qj.1990.

Hoffman, M. J., E. Kalnay, J. A. Carton, and S.-C. Yang, 2009: Use of breeding to detect and explain instabilities in the global ocean. *Geophys. Res. Lett.*, **36**, L12608, doi: 10.1029/2009 GL037729.

Kalnay, E., 2003: *Atmospheric Modeling, Data Assimilation, and Predictability*. Cambridge University Press, 341 pp.

Kalnay, E., and Z. Toth, 1994: Removing growing errors in the analysis cycle. *Tenth Conf. on Numerical Weather Prediction*. Amer. Meteor. Soc., Boston, MA, 212–215.

Kalnay, E., and Z. Toth, 1996: The breeding method. *Proc. the Seminar on Predictability*, ECMWF, 4-8 September 1995. [Available from ECMWF, Shinfield Park, Reading, Berkshire RG29AX]

Li, J. P., and S. H. Wang, 2008: Some mathematical and numerical issues in geophysical fluid dynamics and climate dynamics. *Communications in Computational Physics*, **3**, 759–793.

Li, J. P., and R. Q. Ding, 2011: Temporal-spatial distribution of atmospheric predictability limit by local dynamical analogs. *Mon. Wea. Rev.*, **139**, 3265–3283, doi: 10.1175/MWR-D-10-05020.1.

Lorenz, E. N., 1963: Deterministic nonperiodic flow. *J. Atmos. Sci.*, **20**, 130–141.

Newman, C. E., P. L. Read, and S. R. Lewis, 2003: Breeding vectors and predictability in the Oxford Mars GCM. *First International Workshop on Mars Atmosphere Modelling and Observations*, 13–15 Jan 2003, Granada, Spain.

Norwood, A., E. Kalnay, K. Ide, S.-C. Yang, and C. Wolfe, 2013: Lyapunov, singular and bred vectors in a multi-scale system: An empirical exploration of vectors related to instabilities. *Journal of Physics A: Mathematical and Theoretical*, **46**, 254021, doi: 10.1088/1751-8113/46/25/254021.

Oczkowski, M., I. Szunyogh, and D. J. Patil, 2005: Mechanisms for the development of locally low-dimensional atmospheric dynamics. *J. Atmos. Sci.*, **62**, 1135–1156.

Patil, D. J., B. R. Hunt, E. Kalnay, J. A. York, and E. Ott, 2001: Local low dimensionality of atmospheric dynamics. *Phys. Rev. Lett.*, **86**, 5878–5881.

Toth, Z., and E. Kalnay, 1993: Ensemble forecasting at NMC: The generation of perturbations. *Bull. Amer. Meteor. Soc.*, **74**, 2317–2330.

Toth, Z., and E. Kalnay, 1997: Ensemble forecasting at NCEP and the breeding method. *Mon. Wea. Rev.*, **125**, 3297–3318.

Wolf, A., J. B. Swift, H. L. Swinney, and J. A. Vastano, 1985: Determining Lyapunov exponents from a time series. *Physica D: Nonlinear Phenomena*, **16**, 285–317.

Wolfe, C. L., and R. M. Samelson, 2007: An efficient method for recovering Lyapunov vectors from singular vectors. *Tellus A*, **59**, 355–366.

Yang, S.-C., E. Kalnay, M. Cai, M. Rienecker, G. Yuan, and Z. Toth, 2006: ENSO bred vectors in coupled ocean-atmospheric general circulation models. *J. Climate*, **19**, 1422–1436.

Yang, S.-C., C. Keppenne, M. Rienecker, and E. Kalnay, 2009: Application of coupled bred vectors to seasonal-to-interannual forecasting and ocean data assimilation. *J. Climate*, **22**, 2850–2870.

Young, R. M. B., and P. L. Read, 2008: Breeding and predictability in the baroclinic rotating annulus using a perfect model. *Nonlinear Processes in Geophysics*, **15**, 469–487.